JOURNAL OF Materials CHEMISTRY

Surface and bulk characterisation of titanium–oxo clusters and nanosized titania particles through ^{17}O solid state NMR

Emmanuel Scolan,[a] Claire Magnenet,[b] Dominique Massiot[b] and Clément Sanchez*[a]

[a]*Laboratoire de Chimie de la Matière Condensée – UMR CNRS 7574, Université Pierre et Marie Curie, 4, place Jussieu, 75005 Paris, France. E-mail: clems@ccr.jussieu.fr*
[b]*Centre de Recherches sur les Matériaux à Haute Temperature, 1D Avenue de la Recherche Scientifique, 45071 Orléans Cedex 2, France*

Received 10th May 1999, Accepted 25th June 1999

For the first time, titanium–oxo based nano-objects have been probed using ^{17}O MAS and 3Q-MAS NMR. Three titanium oxo–organo clusters {$[Ti_{12}O_{16}(OPr^i)_{16}]$, $[Ti_{16}O_{16}(OEt)_{32}]$ and $[Ti_{18}O_{22}(OBu^n)_{26}(acac)_2]$}, and monodisperse nanoparticles of titania anatase having 20 and 30 Å oxide core diameters, have been characterised by ^{17}O NMR. This study shows that in titanium oxo-based compounds, the μ_2-O sites are dominated by a significant chemical shift anisotropy, an interaction that is much weaker for the other μ_n-O sites ($n=3$, 4, 5). For all μ_n-O sites ($n=2$, 3, 4 or 5), the ^{17}O NMR linewidths are dominated by chemical shift distribution with a minor contribution from second order quadrupolar broadening. However, depending on the degree of distortion from tetrahedral geometry, the μ_3-O sites can also be sensitive to second order quadrupolar effects. Bulk μ_3-O and surface oxo species (μ_3-O, μ_2-O and acac–Ti) present in titania anatase nanoparticles are identified and clearly assigned. The ratio between bulk and surface species decreases as the particle size is increased. The surface reconstruction of the nanoparticles in the presence of $^{17}OH_2$ enriched moist air, at room temperature, is demonstrated by ^{17}O MAS NMR experiments. From these experiments the μ_3-O, μ_2-O, Ti–OH, acac–Ti and $H_2O\rightarrow$Ti surface species were identified.

Introduction

Sol–gel processes are a method of producing dispersed materials *via* the growth of metal–oxo-polymers in a solvent.[1,2] The chemistry involved in sol–gel processes is based on the hydrolysis and condensation reactions of metallo-organic compounds such as metal alkoxides $[M(OR)_n]$ leading to the formation of metal–oxo polymers. The combination of these metal–oxo polymers can produce bushy structures that pervade the whole volume, forming amorphous gels when these oxo-polymers reach macroscopic sizes, or disordered precipitates when reactions produce dense rather than bushy structures.[1,3] Indeed, amorphous macroscopic networks are not the only possible outcome for such polymerisation reactions. When the polymerised structures do not reach macroscopic sizes, other final states can be obtained, including molecular metal–oxo–organo clusters[4,5] and sols containing nanocrystalline metal oxide particles.[6,7]

Titanium oxide based compounds can be obtained through the controlled hydrolysis of $Ti(OR)_4$ alkoxides, using complexing ligands or protons as inhibitors.[3,6,8–10] The technological importance of titania based materials has been well known for a long time. Indeed, these materials exhibit numerous applications. They can be used as pigments, as powders for catalytic or photocatalytic applications, as colloids and thin films for photovoltaic, electrochromic, photochromic and electroluminescence devices and sensors, as components for antireflecting coatings, as porous membranes for ultrafiltration and even as refractory fibres.[1,11–13]

Amongst these applications, many of the corresponding properties depend on the structure of the TiO_2 phase (mainly anatase, brookite and rutile), and are driven by the nature and the extension of the surface and thus the size of the titania particles. Consequently, it is of primary importance to have effective characterisation tools that can accurately probe the chemical species constituting the bulk and the surface of these titania based nanomaterials.

Contrary to silica based materials for which ^{29}Si MAS NMR techniques are particularly useful and relevant,[1,14] sol–gel derived titanium oxide based materials cannot be routinely probed by NMR experiments performed on the titanium nuclei. Indeed, titanium isotopes carrying a nuclear spin ($^{47}Ti^{IV}$, $^{49}Ti^{IV}$) possess a strong quadrupolar moment that, up to now, makes it difficult to monitor high-resolution solid state titanium NMR[15] experiments. Another possibility, which has been more recently investigated, is to characterise transition metal–oxo polymers by probing oxygen atoms that directly observe the connectivity between different metallic atoms using NMR.[5,9,16–20]

Oxygen is a key constituent of many important oxide based materials. Therefore, amongst the quadrupolar nuclei, ^{17}O ($I=5/2$) is of paramount importance. In addition, oxygen NMR parameters are sensitive to molecular structure and chemical environment, suggesting that direct observation of the ^{17}O spectra has the potential to yield valuable and previously inaccessible information. Oxygen-17 chemical shifts span over a range of *ca.* 1500 ppm and along with quadrupolar coupling parameters provide detailed information on oxygen bonding, solvation, crystallographic symmetry and molecular structure. The main drawback of ^{17}O NMR is its poor sensitivity owing to the low natural abundance of ^{17}O (0.037% natural abundance) and its quadrupolar momentum ($I=5/2$, $Q=-2.63\times10^{-30}$ m^2). However, the quadrupolar interaction broadens the central transition only to second order and the low natural abundance can be overcome by hydrolysing precursors with ^{17}O-enriched water. The relative stability of the C–O bond compared to the Ti–O bond ensures that ^{17}O is efficiently incorporated in the growing Ti–O–Ti oxide network. This strategy has been widely used in the study of the titanium–oxo polymers formed by sol–gel processing.[5,9,18] Indeed, ^{17}O NMR allows for the differentiation of oxygen sites as a function of the number of titanium atoms bonded to them. This work describes the high resolution solid state ^{17}O NMR characterisation of three titanium–oxo–organo clusters {$[Ti_{12}O_{16}(OPr^i)_{16}]$, $[Ti_{16}O_{16}(OEt)_{32}]$ and $[Ti_{18}O_{22}(OBu^n)_{26}(acac)_2]$} as well as monodisperse nanoparticles of titania

anatase having mean oxide network diameters of 20 and 30 Å. The structurally well defined clusters are used as references to classify the dominant magnetic interactions that contribute to the ^{17}O NMR resonances in titanium oxide based materials. For the first time, bulk and surface oxygenated species present in anatase particles are clearly identified and assigned through ^{17}O NMR. Moreover, due to their high surface/bulk ratio, surface reconstruction of the titanium dioxide nanoparticles, occurring at room temperature through exchange reactions with air moisture, is clearly observed.

The methodology presented in the present work opens a vista of opportunities for improving our knowledge of metal oxide surfaces in nanocomposite materials (for example inorganic charges for polymers, pigments, catalysts and photocatalysts, *etc*).

Experimental

Titanium–oxo–alkoxo clusters

$[Ti_{12}O_{16}(OPr^i)_{16}]$, $[Ti_{16}O_{16}(OEt)_{32}]$ and $[Ti_{18}O_{22}(OBu^n)_{26}(acac)_2]$ (acac = acetylacetonate) clusters (Fig. 1) were synthesised following procedures described in the literature.[4,5,9,21,22] $[Ti_{12}O_{16}(OPr^i)_{16}]$ was synthesised by the reaction of 15 g of $Ti(OPr^i)_4$ with 1 equivalent of 20% ^{17}O enriched water in isopropanol (30 ml) in a de Parr bomb at 100 °C for 3 days. After removal of all volatiles, the clusters were isolated and recrystallized overnight from heptane at −20 °C.

$[Ti_{16}O_{16}(OEt)_{32}]$ was obtained after the hydrolysis (0.6 equivalents of 20% ^{17}O enriched water) of 7 ml of $Ti(OEt)_4$ dissolved in 7 ml of anhydrous ethanol. This solution was kept in a bomb at 100 °C for 2 weeks. Crystals were isolated from the solution after slow cooling.

$[Ti_{18}O_{22}(OBu^n)_{26}(acac)_2]$ was prepared by improving a procedure described in the literature.[9,22] Crystals were obtained by adding 0.3 equivalents of Hacac dropwise to $Ti(OBu^n)_4$. The solution was then hydrolysed with a saturated solution of water in butanol (19% w/w) in order to adjust the hydrolysis ratio $Ti:H_2O$ to unity. These crystals were isotopically enriched by using 40% ^{17}O enriched water for their synthesis. The resulting clear solution was then irradiated under a UV beam until the solution became dark green, indicating the presence of Ti^{III} centres. The solution was aged at room temperature and crystals appeared 1–3 days after irradiation. The rotors were filled with the solid clusters using a glove box under an inert atmosphere.

These three clusters were initially characterised by X-ray diffraction. Powder X-ray diffraction patterns were recorded on a Philips diffractometer using θ–2θ Bragg–Brentano reflection geometry and Cu-Kα radiation. Single crystal X-ray data from the literature were used to calculate the corresponding powder X-ray diffraction diagrams using the FullProf program. Good agreement was obtained between experimental diffraction powder patterns and calculated diffractograms. The structures of $[Ti_{12}O_{16}(OPr^i)_{16}]$, $[Ti_{16}O_{16}(OEt)_{32}]$ and $[Ti_{18}O_{22}(OBu^n)_{26}(acac)_2]$ are shown in Fig. 1(a), (b) and (c), respectively.[4,21,22]

The structure of $[Ti_{12}O_{16}(OPr^i)_{16}]$ consists of a cage with pseudo-C_{2h} structure. Half of the Ti atoms are six-coordinate and the remainder are five-coordinate. Each molecule contains two μ_2-O and two μ_3-O ligands that bridge three six-coordinate Ti atoms. The 12 other μ_3-O ligands bridge two five-coordinate Ti atoms and one six-coordinate Ti atom. Each molecule also contains four μ_2-(OPr^i) ligands that bridge two six-coordinate Ti atoms, and 12 terminally-bonded (OPr^i) ligands. The mean size of the oxide core is approximately 9 Å.

The structure of $[Ti_{16}O_{16}(OEt)_{32}]$ consists of two orthogonal blocks of eight TiO_6 octahedra. The 16 titanium atoms are interconnected through three different types of oxygen bridges. Four oxygen atoms are doubly bridging (μ_2-O), eight are triply bridging (μ_3-O) and four are quadruply bridging (μ_4-O). Finally, 16 alkoxo groups are μ_2. The octahedral surroundings are completed by 16 terminal alkoxo groups. The mean size of the oxide core is approximately 12 Å.

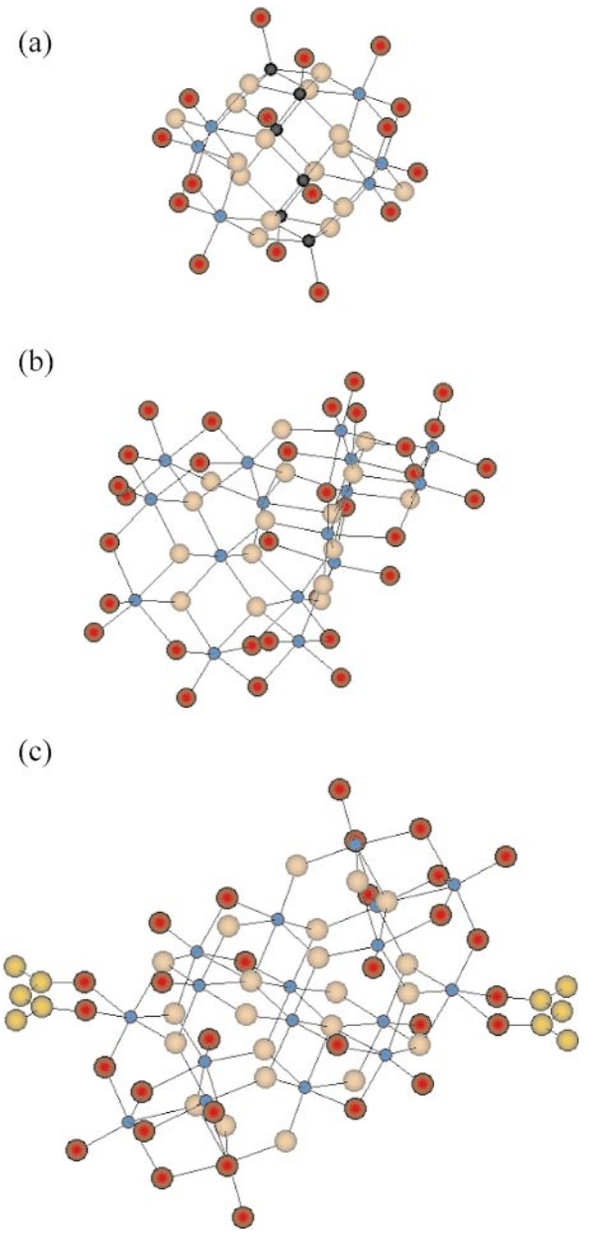

Fig. 1 Molecular structures of (a) $[Ti_{12}O_{16}(OPr^i)_{16}]$, (b) $[Ti_{16}O_{16}(OEt)_{32}]$ and (c) $[Ti_{18}O_{22}(OBu^n)_{26}(acac)_2]$ clusters. For the sake of clarity, only the oxide core is shown. Five- and six-coordinate Ti atoms are represented by black and blue small spheres, respectively. Oxo bridges and O atoms belonging to ligands are represented by white and red spheres, respectively, and C atoms (acac) by green spheres.

The $[Ti_{18}O_{22}(OBu^n)_{26}(acac)_2]$ structure contains 18 titanium atoms in distorted octahedra sharing corners and edges. The '$Ti_{18}O_{22}$' oxide core is surrounded by 26 butoxide groups and two symmetric acac ligands. The titanium oxo metallic core is composed of eight μ_2-O, ten μ_3-O, two μ_4-O and two μ_5-O ligands and the mean size of the oxide core is approximately 15 Å.

$[Ti_{12}O_{16}(OPr^i)_{16}]$, $[Ti_{16}O_{16}(OEt)_{32}]$ and $[Ti_{18}O_{22}(OBu^n)_{26}(acac)_2]$ were also characterised in solution using ^{17}O (Table 1) and $^{13}C\{^1H\}$ NMR spectroscopy. $[Ti_{12}O_{16}(OPr^i)_{16}]$ dissolved in toluene–C_6D_6 (1/1 w/w) showed signals in its 75.47 MHz $^{13}C\{^1H\}$ NMR spectrum (C_6D_6 as internal standard, relative intensities in parentheses) at δ 80.6 (2), 80.4 (4), 80.0 (4), 77.6 (2) and 76.8 (4) in the CH region.

$[Ti_{16}O_{16}(OEt)_{32}]$ dissolved in toluene–C_6D_6 (1/1 w/w) showed in its $^{13}C\{^1H\}$ NMR spectrum, under the same conditions, signals at δ 73.7 (4), 73.3 (4), 72.4 (4), 72.2 (4), 71.6 (4), 71.2 (4), 70.0 (4) and 69.4 (4) in the CH_2 region.

$[Ti_{18}O_{22}(OBu^n)_{26}(acac)_2]$ dissolved in $CDCl_3$ showed signals in its 75.47 MHz $^{13}C\{^1H\}$ NMR spectrum ($CDCl_3$ as internal standard) at δ 79.8 (4), 78.8 (4), 78.1 (4), 76.6 (4), 76.0 (4), 75.6 (4) and 74.7 (2) in the CH_2 region.

These solution NMR results are in excellent agreement with those reported in the literature for $[Ti_{12}O_{16}(OPr^i)_{16}]$,[4] $[Ti_{16}O_{16}(OEt)_{32}]$[5] and $[Ti_{18}O_{22}(OBu^n)_{26}(acac)_2]$,[9] showing that the titanium–oxo cluster structures can be preserved in solution.

Titania nanoparticles

Monodisperse non-aggregated TiO_2 anatase nanoparticles were synthesised using ^{17}O enriched water following a procedure previously described.[6] The key parameter controlling the size of the particles is the initial [acetylacetone(Hacac)]/[metal] complexing ratio A. The size of the nanoparticles can be adjusted by careful tuning of A. The value of A employed was 1 and 4 for the two different sols, X_1 and X_4, synthesised. Characterisation of the solid nanoparticles obtained after drying was carried out by X-ray diffraction, TEM, FTIR, TG-DTA and ^{13}C CP-MAS NMR.[6]

Fig. 2 shows typical XRD patterns recorded for the two dried powders X_1 and X_4. These patterns are characteristic of crystalline particles of TiO_2 anatase. The mean sizes of the titania particles have been fitted from the measured linewidths using the Scherrer relation assuming that the line broadening is essentially due to the size effect. The average diameters, deduced from the full width at half maximum are 30 ± 3 Å and 20 ± 3 Å for complexing A ratios of 1 (X_1) and 4 (X_4), respectively. These values are also consistent with the mean sizes observed by TEM experiments.[6] The inset in Fig. 2 shows a TEM micrograph of nanoparticles of X_1. Electron diffraction performed on these particles shows that the oxide phase corresponds to crystalline titania anatase and the lattice planes correspond to the (101) orientation (d_{101} = 3.52 Å).

To better understand the hydrolysis process, we synthesised X_{1s} and X_{4s} samples using natural water for the hydrolysis step. After drying in air at 100 °C, the dried xerosols were kept in a closed vessel for one month in the presence of ^{17}O enriched moist air. Samples were then dried under a moderate argon flow.

NMR experiments

^{17}O ($I=5/2$) NMR spectra consist of a superposition of the $2I=5$ single quantum transitions, the central $<1/2,-1/2>$ transition and the symmetric $<\pm3/2,\ \pm1/2>$ and $<\pm5/2,\ \pm3/2>$ external transitions. The spectra are dominated by chemical shift anisotropy (CSA) and quadrupolar interaction terms. Chemical shift anisotropy is due to the shielding of the principal field by valence electrons and directly characterises the bonding state and geometry of the oxygen site. The quadrupolar interaction is due to the interaction of the nuclear quadrupolar momentum with the electric field gradient at the nucleus site. In solid state powders, this gives rise to first order spreading or external transitions and possibly (when strong enough) to second order broadening of the central transition. This second order broadening is proportional to the inverse of the principal field and cannot be removed by conventional acquisition of a one-dimensional spectrum under magic angle spinning alone. It can be averaged out by combining magic angle spinning (MAS) and evolution of the indirectly observed multiple quantum (typically triple quantum) coherences in the recently described two-dimensional multiple quantum experiment (MQ-MAS).[23–26] These experiments provide a unique way of separating out the respective influences of chemical shift distribution and quadrupolar interaction on the broadening observed in one-dimensional experiments.

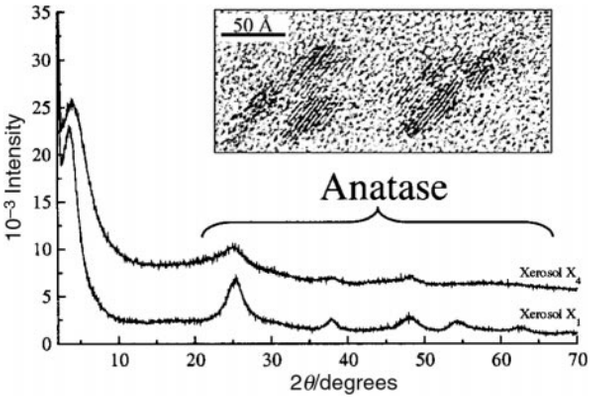

Fig. 2 XRD patterns corresponding to X_1 and X_4 xerosols. The inset corresponds to a TEM micrograph of X_1 nanoparticles.

The solid state high resolution ^{17}O NMR spectra presented below were acquired on Bruker DSX solid state NMR spectrometers with double bearing magic angle probe-heads allowing a spinning rate of up to 15 kHz with 4 mm zirconia rotors. Most of the experiments were acquired at 9.4 T (^{17}O Larmor frequency 54.25 MHz). When necessary, additional spectra have been acquired at a lower principal field of 7.0 T (^{17}O Larmor frequency 40.69 MHz) to confirm the existence or otherwise of field dependent second order quadrupolar broadening. For solid state and solution experiments, the ^{17}O resonance of tap water was taken as the reference at $\delta=0$.

^{17}O MAS NMR. One dimensional MAS ^{17}O spectra were acquired using a simple one pulse excitation sequence while spinning at typically 12 kHz with a small pulse angle (typically $\pi/12$) and recycle delays of 1 to 5 s to ensure a possible quantitative interpretation of the obtained spectra.[27,28] Application of proton decoupling during acquisition does not lead to observable modification of the obtained spectrum. The rolling sinc base line, due to dead time truncation, has been corrected according to a previously described protocol. For some samples additional spectra were obtained on static spectra using echo sequences to provide an unambiguous phasing of the obtained spectrum and identification of the static shapes of the individual contributions resolved in the MAS spectra. Owing to the complexity of the ^{17}O spin system, which can involve large chemical shifts and quadrupolar interactions, echo experiments result in possibly non-quantitative spectra and no attempt was made to systematically use these echo techniques. The final processing and fitting of the resulting spectra was performed using a modified version of the Bruker Winfit program. The values reported below for the chemical shift anisotropy and quadrupolar interaction considered all the spectra acquired under different conditions for each sample. A striking result of this study is the fact that, for all the reference clusters, the quadrupolar interaction remains small whereas chemical shift anisotropy has a tendency to become large. Indeed, the chemical shift anisotropies that we measured for μ_2-O sites, seem to be the highest values reported so far. When dealing with less ordered systems such as nanoparticles, it becomes difficult or impossible to identify, in a simple 1D experiment at one field, the source of broadening which may be due to chemical shift distribution or quadrupolar interaction. Additional experiments have been carried out on one sample at very high fields (500 and 800 MHz) and spinning rates (25 to 35 kHz) to better understand the observed spectra.

^{17}O MQ-MAS NMR. As mentioned above, the MQ-MAS experiment opens a way of removing the second order quadrupolar broadening in two-dimensional experiments. It also provides a unique way of separating the parameters such as chemical shift anisotropy and/or quadrupolar factors. The 3Q-MAS experiments presented below were acquired using a simple two-pulse excitation with hyper-complex acquisition, giving a final pure phase two-dimensional spectrum. Owing to the sharp lines in the indirectly detected F1 dimension and limited sensitivity (960 scans per slice), the acquisition of a complete two-dimensional data-set with fully resolved isotropic dimension would typically take 5 to 6 days. In order to achieve reasonable acquisition times, rotor synchronised data acquisition was applied in the isotropic F1 dimension to shorten the acquisition time.[29] This shortens the acquisition to slightly more than one day but results in folding back of lines in the isotropic dimension. The final data set was then processed so as to restore a large enough isotropic dimension by introducing three pairs of null slices between each pair of acquired slices. The resulting spectra have a four times larger isotropic dimension in which each line is replicated four times (lines marked by an asterisk on figures). Owing to limited second order quadrupolar broadening, the procedure made it possible to acquire data without introducing any artificial line overlapping. In the figures below, the line correlating chemical shifts in both dimensions (slope −17/31) has been added for clarity.

Results and discussion

Titanium oxo–alkoxide clusters

The ^{17}O MAS NMR spectra recorded on the three titanium oxo-alkoxide clusters {$[Ti_{12}O_{16}(OPr^i)_{16}]$, $[Ti_{16}O_{16}(OEt)_{32}]$ and $[Ti_{18}O_{22}(OBu^n)_{26}(acac)_2]$} are presented in Fig. 3. An excellent resolution of all the μ_n-O bridges is clearly observed. Chemical shift values, linewidths and normalised integrated intensities obtained from the simulation of all the spectra are reported in Table 1. The chemical shift values for a given set of μ_n-O species are similar to those reported in solution (Table 1). A good agreement is obtained between the abundance of a given set of μ_n-O species determined from X-ray data and the integrated resonances. Consequently, the ^{17}O resonances corresponding

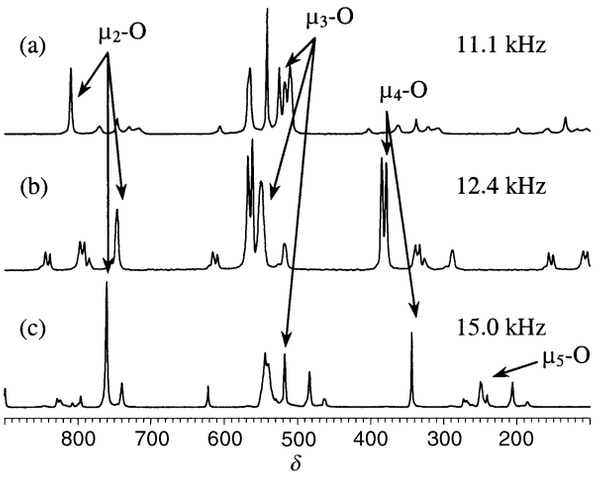

Fig. 3 ^{17}O MAS NMR spectra recorded at 54.25 MHz for (a) $[Ti_{12}O_{16}(OPr^i)_{16}]$, (b) $[Ti_{16}O_{16}(OEt)_{32}]$ and (c) $[Ti_{18}O_{22}(OBu^n)_{26}(acac)_2]$ clusters. Arrows indicate the central transitions.

to the four different types of titanium oxo bridges (μ_2-O, μ_3-O, μ_4-O and μ_5-O) present in these clusters can be clearly assigned according to their different crystallographic structures.[4,21,22] The evolution of the ^{17}O MAS NMR spectra of the three clusters recorded at different spinning rates (from 3 to 15 KHz), clearly show an important spreading of the μ_2-O magnetisation in many spinning side bands. As an example, the data for the $[Ti_{16}O_{16}(OEt)_{32}]$ cluster is shown in Fig. 4. For low spinning rates, the intensity of some spinning bands can become higher than that of the isotropic resonance. This spreading of the spinning bands intensities is strongly asymmetric with respect to the isotropic resonance. This is a typical feature of NMR resonances under the influence of strongly anisotropic interactions with predominating chemical shift anisotropy. This feature is also observed for the other μ_2-O sites within the different titanium oxo clusters in which the chemical shift anisotropy parameter $\Delta\sigma$ spans the range 500–650 ppm (Table 1). The chemical shift anisotropy is much weaker for the characteristic resonances of μ_3-O, μ_4-O and μ_5-O species as confirmed through ^{17}O MAS NMR experiments performed at 47.69 and 54.25 MHz, ^{17}O 3Q-MAS NMR, ^{1}H

Table 1 Magnetic ^{17}O parameters obtained for $[Ti_{12}O_{16}(OPr^i)_{16}]$, $[Ti_{16}O_{16}(OEt)_{32}]$, $[Ti_{18}O_{22}(OBu^n)_{26}(acac)_2]$ clusters and titania nanoparticles (X_1 and X_4 correspond to samples containing titania nanoparticles having mean diameters of 30 and 20 Å, respectively)[a]

Titanium oxo-entity	$\delta_{solution}$	$\delta_{solid\ state}$	Solid state linewidth/Hz	Integration	Assignment	$\Delta\sigma_{MAS}$/ppm	η_{MAS}	$\Delta\nu_Q$/kHz	η_Q
$Ti_{12}O_{16}(OPr^i)_{16}$	817	809	147	2	μ_2-O	185	0.45		
	564	565	293	4	μ_3-O				
	538	541	98	2	μ_3-O				
	522	524	174	2	μ_3-O				
	517	517	215	2	μ_3-O				
		510	282	4	μ_3-O				
$Ti_{16}O_{16}(OEt)_{32}$	750	746	235	4	μ_2-O	597[b] 620[c]	0.45[b] 0.20[c]		
	563	567	227	2	μ_3-O				
		561	153	2	μ_3-O				
	555	554		4	μ_3-O			236	0.5
	383	384	160	2	μ_4-O				
		378	157	2	μ_4-O				
$Ti_{18}O_{22}(OBu^n)_{26}(acac)_2$	755/753	755	147	6	μ_2-O	554	0.55		
	738	738	176	2	μ_2-O	610	0.60		
	545	545		8	μ_3-O			302	0.4
	508	810	137	2	μ_3-O				
	340	340	85	2	μ_4-O				
	247	245	202	2	μ_5-O				
TiO_2 nanoparticles		740	5041		μ_2-O	694	0.00		
		561	2060	(*)	μ_3-O				
		541	4307		μ_3-O				
		370	4319		acac				

[a]The NMR surface/bulk ratios were calculated from the resonances integrations (I) as follows: $(I_{\mu_2\text{-O}} + I_{\mu_3\text{-O}}(\delta\ 541) + I_{acac})/I_{\mu_3\text{-O}}(\delta\ 541)$ gives 49/51 for X_1 and 67/33 for the X_4 xerosol. [b]MAS. [c]Static.

decoupled static ^{17}O NMR and simple echo static ^{17}O NMR recorded on the clusters.

As an example, the data obtained for the $[Ti_{16}O_{16}(OEt)_{32}]$ cluster are illustated in Fig. 5 and 6. The ^{17}O 3Q-MAS NMR spectrum exhibits correlation spots corresponding to μ_2-O and μ_3-O, μ_4-O species. All of these spots are located close to the line with a slope of $-17/31$ and scarcely deviate from this axis. This behaviour is characteristic of a weak chemical shift distribution and negligible second order quadrupolar broadening. However the resonance located at δ 553 (characteristic of μ_3-O species) is slightly right shifted with respect to the slope $-17/31$ and is smeared out horizontally. This is the characteristic feature of an ^{17}O site with a significant second order quadrupolar broadening.

The ^{1}H decoupled static ^{17}O NMR spectrum is shown in Fig. 6. It is evident that the line shape and anisotropy of the μ_3-O and μ_4-O species are qualitatively different from those of the μ_2-O species. They have been fitted by taking into account both chemical shift and quadrupolar anisotropy. The magnetic parameters obtained through simulation are gathered in Table 1. These values of $\Delta\sigma$ and η are close to those obtained from simulation of the MAS spectra using the model proposed by Hertzfeld and Berger,[30] and confirm two main points.

(i) The ^{17}O NMR resonances corresponding to μ_2-O species are dominated by a strong chemical shift anisotropy ($\Delta\sigma \approx 650$ ppm) and a low asymmetric parameter ($\eta \approx 0.2$), translating a nearly axial symmetry of the μ_2-O environment.

(ii) The quadrupolar anisotropy is weak for all μ_n-O species except for the μ_3-O species located at δ 555 which are characterised by broader linewidths.

As previously reported, the quadrupolar anisotropy should increase with the covalent character of the chemical O–M bonds.[31] Thus an increase in the component of the linewidth corresponding to this interaction is expected with a decrease in oxygen connectivity. However the main difference in line broadening is observed for μ_3-O species located at δ 555 (with respect to other μ_3-O species located at δ 567/571) and can be correlated to the geometry of the titanium oxo sites. The field gradient should be higher when distortion from tetrahedral symmetry[31] occurs, *i.e.* when some flattening of the tetrahedron occurs leading μ_3-O planar species.

NMR data for the $[Ti_{18}O_{22}(OBu^n)_{26}(acac)_2]$ cluster exhibit signals due to μ_2-O species dominated by a strong chemical shift anisotropy and μ_4-O and μ_5-O species with weak chemical shift and quadrupolar anisotropy. The resonances corresponding to μ_3-O species can be split into two components: those with small linewidths (*ca.* 140 Hz) located at δ 508 that integrate for two oxygen atoms, and those characterised by a broader resonance located at δ 545 that integrate for eight oxygen atoms. The line width of the broad line located at δ 545 decreases when the magnetic field is increased and confirms that it is dominated by second order quadrupolar effects, as is evident from a 3Q-MAS experiment. Moreover taking into account the geometry obtained from crystallographic data, a straightforward assignment can be proposed: eight oxygen sites exhibit a planar geometry (the sum of the Ti–O–Ti angles is close to 360°, *i.e.* 357–354°) while two are in a weakly distorted tetrahedral oxygen environment (the sum of the Ti–O–Ti angles are close to 312°).

On this basis, the broad resonance located at δ 545 can be assigned to planar μ_3-O species while the sharper signal located at δ 508 can be assigned to tetrahedral μ_3-O species. Assignments can be extended to the other clusters. Indeed, the resonances of the μ_3-O species present in $[Ti_{12}O_{16}(OPr^i)_{16}]$ are quite sharp, in agreement with the fact that in this cluster all of the μ_3-O have a weakly distorted tetrahedral geometry. Moreover, for the $[Ti_{16}O_{16}(OEt)_{32}]$ cluster, in agreement with crystallographic data, the broad resonance located at δ 555 (integrating for four oxygen atoms) and the sharper signals located at δ 561 and 567 (each integrating for two oxygen atoms) should correspond to planar and tetrahedral μ_3-O species, respectively.

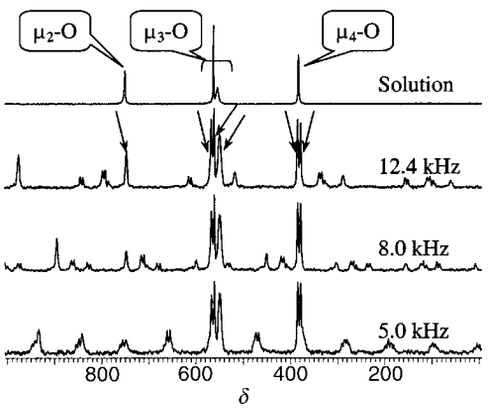

Fig. 4 ^{17}O MAS NMR spectra recorded at 54.25 MHz for the $[Ti_{16}O_{16}(OEt)_{32}]$ cluster at different spinning rates. Arrows indicate the central transitions.

Titania nanoparticles

The ^{17}O MAS NMR spectra of xerosols of X_1 (average diameter of the TiO_2 anatase core $= 30 \pm 3$ Å) and X_4 (average diameter of the TiO_2 anatase core $= 20 \pm 3$ Å) nanoparticles are shown in Fig. 7. Recording of the spectra at different spinning rates from 3 to 35.5 kHz and at different fields (40.69 MHz, 54.25 MHz, 108.50 MHz) indicates the presence of three different sets of ^{17}O resonances located at δ *ca.* 740, 550 and 370. From comparison with spectra obtained at very different fields (500 and 800 MHz) and spinning rates (25 to 35 kHz), it is clearly apparent that the linewidth and the shape of these three resonances are not modified upon increasing the magnetic field. This indicates that the line broadening of the central transitions is not dominated by quadrupolar interaction but by a chemical shift distribution.

The most deshielded resonance (δ *ca.* 740) is characteristic of μ_2-O species being located in the same region as for μ_2-O sites in titanium–oxo clusters, and displaying a significant chemical shift anisotropy ($\Delta\sigma \approx 690$ ppm, $\eta \approx 0$).

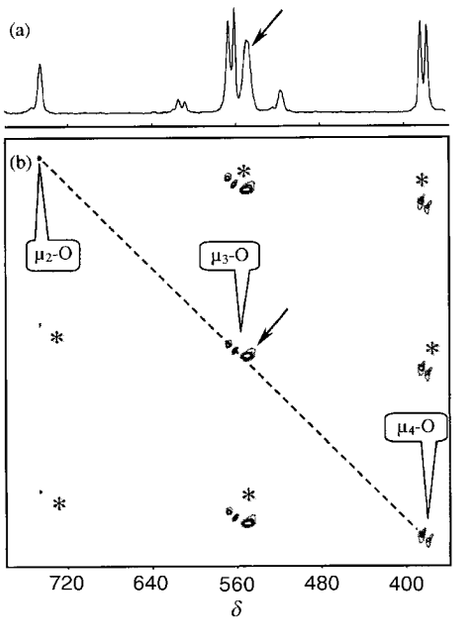

Fig. 5 ^{17}O (a) MAS and (b) 3Q-MAS NMR spectra recorded at 54.25 MHz for the $[Ti_{16}O_{16}(OEt)_{32}]$ cluster. Asterisks indicate replication of the on-diagonal signals and the dashed line is the $-17/31$ slope correlating the two dimensions. The only second order broadened component (marked by an arrow) is of μ_3-O type.

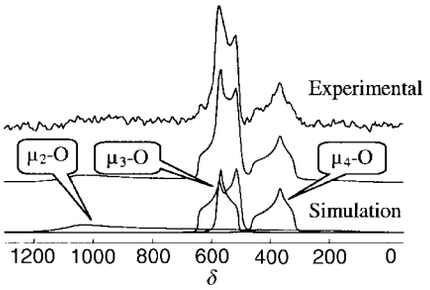

Fig. 6 ^{17}O NMR static spectrum recorded at 54.25 MHz of the $[Ti_{16}O_{16}(OEt)_{32}]$ cluster. Simulated spectra are shown beneath the experimental spectrum.

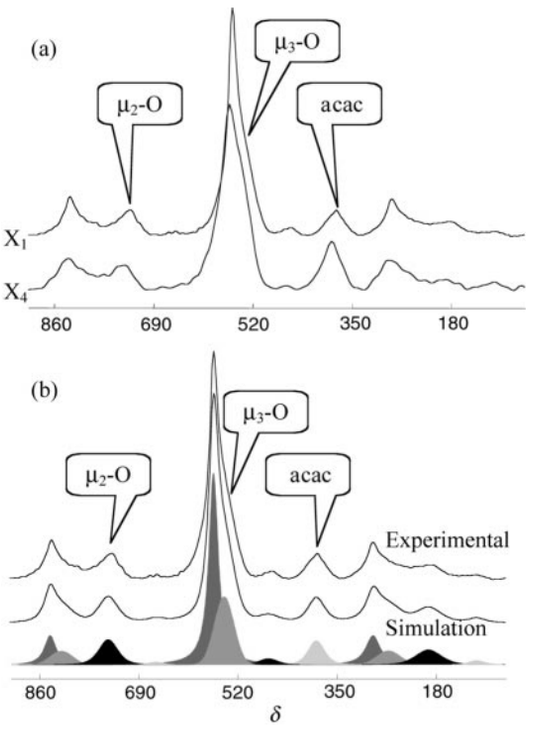

Fig. 7 (a) ^{17}O MAS NMR spectra recorded at 54.25 MHz for X_1 and X_4 xerosols containing titania nanoparticles and (b) a comparison with the simulated spectrum for the X_1 xerosol.

The resonance located at high field, the relative intensity of which increases with ratio *A*, corresponds to acetylacetonate groups bonded to titanium atoms ($\delta_{Ti-O(acac)} = 370$). As previously reported, this ^{17}O resonance results from isotopic ^{17}O-exchange between enriched H_2O and the acetylacetone during hydrolysis.[9,32]

The most intense resonance the maximum of which is located at δ *ca.* 556 corresponds to μ_3-O species. Its asymmetric shape may result either from quadrupolar interaction or from a chemical shift distribution. However, the fact that no sharpening is observed when the magnetic field is increased to 18.8 T suggests that this shape arises from different chemical shifts with the linewidth dominated by chemical shift anisotropy.

Assignments were confirmed by ^{17}O 3Q-MAS NMR experiments recorded on the X_1 sample (Fig. 8). The μ_3-O species are characterised by correlation spots that are located very close to the line with a slope of $-17/31$. A spreading of the correlation spot is also observed along this axis. This behaviour is characteristic of a resonance dominated by a distribution of chemical shifts. The very small spreading of the μ_3-O spot observed along the 10/31 direction may be due to a broadening by weak second order quadrupolar effects. On the basis of the absence of a field effect and ^{17}O 3Q-MAS NMR results, the shape of this resonance can be considered as being due to a superposition of two different components; an intense sharp signal at δ 561 and a broad shoulder at δ *ca.* 541.

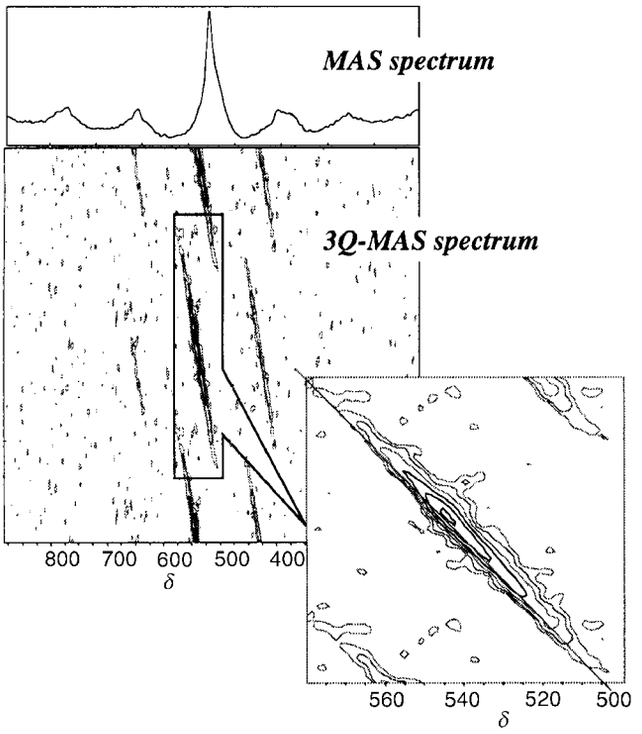

Fig. 8 ^{17}O 3Q-MAS NMR spectra of the X_1 xerosol recorded at 54.25 MHz (spinning rate 8.2 kHz) within the μ_3-O chemical shift range. The line is the $-17/31$ slope correlating the two dimensions.

The results of the best fit obtained for the ^{17}O MAS NMR spectra of the X_1 and X_4 samples are given in Table 1. The relative intensity of the shoulder located at δ 541 increases from X_1 to X_4, *i.e.* when the surface to volume ratio increases. This result aids assignment as confirmed below by water adsorption experiments monitored *via* ^{17}O NMR.

In agreement with the published literature,[18] the most intense resonance located at δ 561 corresponds to bulk anatase μ_3-O species, while the broader line located at δ 541 is assigned to μ_3-O species located at the surface of the anatase particles. The observed broadening may result from quadrupolar anisotropy arising from the distorted surface site as well as a chemical shift distribution.

A model of the titanium oxide core of TiO_2 anatase nanoparticles obtained using the 'CrystalMaker' software allows the calculation of the number of bulk and surface titanium and oxygen atoms for particles of different sizes. Fig. 9 illustrates a plot of the number of metal atoms (surface, bulk, surface + bulk) *versus* the mean size of TiO_2 anatase particles. It is interesting to observe (Table 1) that the calculated relative amount of surface species (broad μ_3-O, μ_2-O and acac-O–Ti) compared to bulk species (sharp μ_3-O) (from NMR data surface/bulk ratios of 49/51 and 67/33 for X_1 and X_4 respectively) are in excellent agreement with the surface to bulk ratios obtained through simulation (surface/bulk ratios of 48/52 and 67/33 are obtained for anatase particles with mean diameters of 30 and 20 Å, respectively).

Prior to treatment with ^{17}O enriched moist air, non-enriched xerosols are ^{17}O NMR silent. By contrast, xerosols of nanoparticles X_{1s} and X_{4s}, which were synthesised using non-enriched water (^{17}O in natural abundance) and subsequently aged using ^{17}O enriched moist air, present several ^{17}O NMR resonances in their ^{17}O MAS NMR spectra recorded at 54.25 MHz, shown in Fig. 10. The sharp resonance located at δ 561 previously assigned to μ_3-O bulk anatase species is ^{17}O

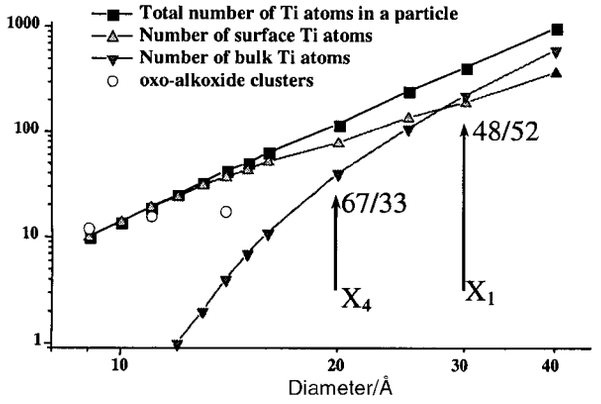

Fig. 9 Plot of the number of titanium atoms *versus* the mean size of titania anatase nanoparticles. Simulation obtained using the 'CrystalMaker' program. 67/33 and 48/52 represent the calculated surface/bulk atom ratios for titania anatase particles having 20 and 30 Å mean diameter, respectively.

NMR silent within experimental sensitivity. However, the ^{17}O MAS NMR spectra exhibit five sets of different resonances which can be assigned as follows.

A resonance showing many spinning bands, located at δ 740 is assigned to surface μ_2-O sites. A broad resonance located at δ 541 is assigned to surface μ_3-O species and that at δ 370 to surface acac species. Two other weaker resonances at δ 195 and -65 in the X_{1s} and X_{4s} spectra were not detectable in the spectra of the X_1 and X_4 samples which were ^{17}O enriched directly during synthesis.

Previous studies on metallic aquo–hydroxo compounds[33,34] have shown that the chemical shift of terminal water bound to a 3d metal acting as a Lewis base adduct ($H_2O\rightarrow M$) is located at negative values [$\delta(H_2O\rightarrow Mo(III))$ -40] with respect to the free water resonance (δ 0). Following from this, the δ -65 resonance can be assigned to solvated metallic sites such as $H_2O\rightarrow Ti(IV)$. As previously reported from ^{17}O CP experiments,[35] the other resonance located at δ 195 is in the domain

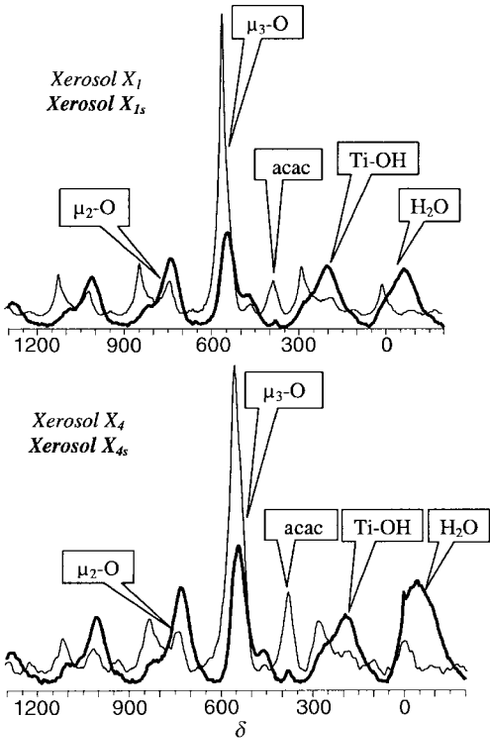

Fig. 10 ^{17}O MAS NMR spectra recorded at 54.25 MHz of X_{1s} and X_{4s} xerosols (bold lines) compared to those of X_1 and X_4 xerosols, respectively.

expected for Ti–OH groups. Moreover a polycationic Mo(III)–hydroxo compound in water shows a resonance at δ 124 assigned to μ_2-OH species. On this basis we assign the resonance located at δ 195 to Ti–OH species. These two species were not detected for the X_1 and X_4 samples, probably because these samples were exposed to natural moist air during drying. This short period is probably sufficient to exchange the enriched $Ti–^{17}OH$ and $Ti\leftarrow{}^{17}OH_2$ species for corresponding non-enriched groups.

These experiments clearly demonstrate that surface reconstruction of TiO_2 anatase particles can occur under mild conditions. On the basis of this ^{17}O NMR study the oxygenated species present in the bulk and at the surface of the titania anatase nanoparticles can be represented by the partial schematic structure shown in Fig. 11. The presence of *p*-toluenesulfonate species in the solvation sphere of the nanoparticles is supported by a previously reported ^{13}C NMR study.[10]

Conclusions

To the best of our knowledge, for the first time, well defined titanium oxide based nano-objects have been characterised by solid state ^{17}O NMR. This study, concerning titanium–oxo nano-objects, clearly shows that μ_2-O sites are characterised by a significant chemical shift anisotropy while this is quite small for μ_3-O, μ_4-O and μ_5-O sites. For μ_4-O and μ_5-O sites line broadening is due to a chemical shift distribution with only a minor contribution from second order quadrupolar interaction (SOQI). However, depending on the μ_3-O site geometry, the line broadening of the ^{17}O NMR linewidth is affected by SOQI. Broader linewidths were assigned to pseudo-planar μ_3-O species, while sharper resonances were assigned to μ_3-O species in close to tetrahedral geometry.

The surface and bulk species present on synthesised TiO_2 anatase nanoparticles have been characterised. They consist of μ_3-O bulk species and μ_3-O, μ_2-O and acac surface species with characteristic ^{17}O NMR resonances at δ 561, 541, 740 and 370, respectively. These assignments are confirmed through monitoring, *via* ^{17}O NMR, of the surface reconstruction of the TiO_2 nanoparticles. This reconstruction occurring at room temperature under mild conditions points to the presence of two other surface species, Ti–OH and $H_2O\rightarrow Ti$, the characteristic ^{17}O NMR resonances of which are located at δ 195 and -65, respectively. Such surface modification is of paramount importance for nano-objects or highly porous solids (materials with very high surface to volume ratio) and may have drastic influences on their catalytic and photocatalytic properties.

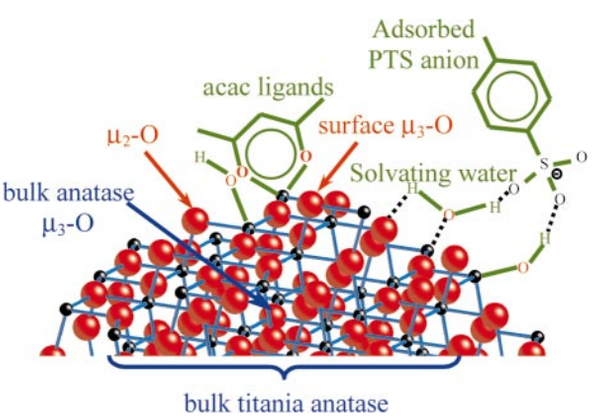

Fig. 11 Schematic representation of ^{17}O species, identified through ^{17}O NMR, present in the bulk and at the surface of the titania nanoparticles. Ti atoms are represented by small black spheres and O atoms by large red spheres. The presence of *p*-toluenesulfonate molecules close to the surface is in agreement with ^{13}C NMR data reported in the literature.[10]

Acknowledgements

We would like to acknowledge Jocelyne Maquet for her help with NMR measurements, Claude Magnier for his scientific interest in this study, and the French Minister of Research and Rhodia S.A. for financial support. We thank Stefan Steuernagel and Hans Forster (Bruker Karlsruhe) for the access provided to very high field experiments. Special thanks are due to Gabbo's for providing an inspiring atmosphere.

References

1 C. J. Brinker and G. W. Scherrer, *Sol–Gel Science: the Physics and Chemistry of Sol–Gel Processing*, Academic Press, San Diego, 1990.
2 J. Livage, M. Henry and C. Sanchez, *Prog. Solid State Chem.*, 1988, **18**, 259.
3 M. Kallala, C. Sanchez and B. Cabane, *Phys. Rev. E*, 1993, **485**, 3692.
4 V. W. Day, T. A. Eberspacher, W. G. Klemperer and C. W. Park, *J. Am. Chem. Soc.*, 1993, **115**, 8469.
5 V. W. Day, T. A. Eberspacher, W. G. Klemperer, C. W. Park and F. S. Rosenberg, *J. Am. Chem. Soc.*, 1991, **113**, 8190.
6 E. Scolan and C. Sanchez, *Chem. Mater.*, 1998, **10**, 3217.
7 A. Chemseddine and T. Moritz, *Eur. J. Inorg. Chem.*, 1999, **2**, 235.
8 C. Sanchez, J. Livage, M. Henry and F. Babonneau, *J. Non-Cryst. Solids*, 1988, **100**, 65.
9 J. Blanchard, S. Barboux-Doeuff, J. Maquet and C. Sanchez, *New J. Chem.*, 1995, **19**, 929.
10 B. E. Yoldas, *J. Mater. Sci.*, 1986, **21**, 1086.
11 B. O'Regan and M. Grätzel, *Nature*, 1991, **353**, 737.
12 K.-N. P. Kumar, K. Keizer, A. J. Burggraaf, T. Okubo, H. Nagamoto and S. Morooka, *Nature*, 1992, **358**, 48.
13 T. Gerfin, M. Grätzel and L. Walder, *Prog. Inorg. Chem.*, 1997, **44**, 345.
14 J. C. Pouxviel, J. P. Boilot, J. C. Beloeil and J. Y. Lallemand, *J. Non-Cryst. Solids*, 1987, **89**, 345.
15 T. J. Bastow, M. A. Gibson and C. T. Forwood, *Solid State NMR*, 1998, **12**, 201.
16 T. H. Walter and E. Oldfield, *J. Phys. Chem.*, 1989, **93**, 6744.
17 T. H. Walter, G. L. Turner and E. Oldfield, *J. Magn. Reson.*, 1988, **76**, 106.
18 T. J. Bastow, A. F. Moodie, M. E. Smith and H. J. Whitfield, *J. Mater. Chem.*, 1993, **3**, 697.
19 P. J. Dirken, M. E. Smith and H. J. Whitfield, *J. Phys. Chem.*, 1995, **99**, 395.
20 P. J. Dirken, S. C. Kohn, M. E. Smith and E. R. H. van Eck, *Chem. Phys. Lett.*, 1997, **266**, 568.
21 R. Schmid, A. Mosset and J. Galy, *J. Chem. Soc., Dalton Trans.*, 1991, 1999.
22 P. Toledano, M. In and C. Sanchez, *C. R. Acad. Sci. Paris Sér. II*, 1991, **313**, 1247.
23 L. Frydman and J. S. Harwood, *J. Am. Chem. Soc.*, 1995, **117**, 5367.
24 A. Medek, J. S. Harwood and L. Frydman, *J. Am. Chem. Soc.*, 1995, **117**, 12779.
25 C. Fernandez and J. P. Amoureux, *Chem. Phys. Lett.*, 1995, **242**, 449.
26 D. Massiot, B. Touzo, D. Trumeau, J. P. Coutures, J. Virlet, P. Florian and P. J. Grandinetti, *Solid State NMR*, 1996, **6**, 73.
27 D. Fenzke, D. Freude, T. Fröhlick and J. Haase, *Chem. Phys. Lett.*, 1984, **111**, 171.
28 D. Massiot, C. Bessada, J. P. Coutures and F. Taulelle, *J. Magn. Reson.*, 1990, **90**, 231.
29 D. Massiot, *J. Magn. Reson. A*, 1996, **122**, 240.
30 J. Herzfeld and A. E. Berger, *J. Chem. Phys.*, 1980, **73**, 6021.
31 S. Schramm and E. Oldfield, *J. Am. Chem. Soc.*, 1984, **106**, 2502.
32 J. Blanchard, M. In, B. Schaudel and C. Sanchez, *Eur. J. Inorg. Chem.*, 1998, **1**, 1115.
33 M. Åberg and J. Glaser, *Inorg. Chim. Acta*, 1993, **206**, 53.
34 D. T. Richens, L. Helm, P. A. Pittet and A. E. Merbach, *Inorg. Chim. Acta*, 1987, **132**, 85.
35 J. Blanchard, C. Bonhomme, J. Maquet and C. Sanchez, *J. Mater. Chem.*, 1998, **8**, 985.

Paper 9/03714D